

Preferred Sites of Exocytosis and Endocytosis Colocalize during High- But Not Lower-Frequency Stimulation in Mouse Motor Nerve Terminals

Michael A. Gaffield,¹ Lucia Tabares,² and William J. Betz¹

¹Department of Physiology and Biophysics, University of Colorado Denver, Anschutz Medical Campus, Aurora, Colorado 80045, and ²Department of Medical Physiology and Biophysics, School of Medicine, University of Seville, 41009 Seville, Spain

The spatial relationship of exocytosis and endocytosis in motor nerve terminals has been explored, with varied results, mostly in fixed preparations and without direct information on the utilization of each exocytic site. We sought to determine these spatial properties in real time using synaptopHluorin (spH) and FM4-64. Earlier we showed that nerve stimulation elicits the appearance of spH fluorescence hot spots, which mark preferred sites of exocytosis. Here we show that nerve stimulation in the presence of the styryl dye FM4-64 evokes hot spots of FM4-64 fluorescence. Their size, density, and rate of appearance are similar to the spH hot spots, but their rate of disappearance after stimulation was much slower ($t_{1/2} \sim 9$ min vs ~ 10 s for spH hot spots), consistent with FM4-64 spots identifying bulk endocytosis and subsequent slow intracellular dispersion of nascent vesicles. Simultaneous imaging of both fluorophores revealed a strong colocalization of spH and FM4-64 spots, but only during high (100 Hz) stimulation. At 40 Hz stimulation, exocytic and endocytic spots did not colocalize. Our results are consistent with the hypothesis that hot spots of endocytosis, possibly in the form of bulk uptake, occur at or very near highly active exocytic sites during high-frequency stimulation.

Introduction

During synaptic transmission at the neuromuscular junction (NMJ), dozens of synaptic vesicles fuse simultaneously with the motor nerve terminal membrane. To maintain a supply of synaptic vesicles, the nerve terminal recovers membrane from the surface via endocytosis [for review, see Wu et al. (2007) and Smith et al. (2008)]. Electron microscopic snapshots of nerve terminals have revealed different modes of endocytosis, including single vesicle retrieval via clathrin-dependent endocytosis (Ceccarelli et al., 1973; Heuser and Reese, 1973; Takei et al., 1996), and uptake of large cisternae or endosomes, which slowly bud synaptic vesicles (Koenig and Ikeda, 1989; Takei et al., 1996; Richards et al., 2000; Teng and Wilkinson, 2000; Holt et al., 2003) [cisternae may maintain a small connection with the plasma membrane (Gad et al., 1998)]. This latter form, often referred to as bulk endocytosis, occurs predominantly during periods of intense activity when a large amount of membrane is added to the surface (Ceccarelli et al., 1972; Heuser and Reese, 1973) [see also Xu et al. (2002) at the mouse NMJ] and may arise from sites enriched in endocytic proteins (Estes et al., 1996). In CNS

nerve terminals, bulk endocytosis is activated immediately with intense stimulation (Clayton et al., 2008), but at the snake NMJ, bulk uptake can occur independently of stimulation levels (Teng et al., 2007).

Signs of extensive endocytosis were first noted toward terminal edges, where nerve, muscle, and Schwann cell membranes converge, far away from exocytic sites (Heuser and Reese, 1973). A later report suggested that endocytosis locations may have no spatial preference (Miller and Heuser, 1984). More recently, spatial locations of endocytic sites have been proposed to emerge in close proximity to exocytic sites at the NMJ (Roos and Kelly, 1999; Teng and Wilkinson, 2000).

We sought to address the degree of colocalization of exocytic and endocytic sites in real time in living motor nerve terminals during different stimulation intensity levels. For localizing exocytic sites, we stimulated motor nerve terminals from a mouse expressing synaptopHluorin (spH) (Miesenböck et al., 1998; Ng et al., 2002; Tabares et al., 2007), which produces spH spots on the terminal surface. We recently showed that spH moves out of, not into, spots after stimulation, thereby providing strong evidence that the spots are exocytic in origin (Gaffield et al., 2009). Here we report observing similar FM4-64 spots when the dye was present during stimulation. FM dyes, used mostly to label endosomes (Betz et al., 1992, 1996), can also reveal sites of exocytosis (Smith and Betz, 1996) because unlabeled membrane added to the surface by exocytosis adsorbs FM dye from solution (FM dye in solution remains nonfluorescent). However, while spH spots disappear quickly after stimulation ends (due to internalization and reacidification of endosomes, which quenches the spH fluorescence), FM4-64 fluorescence, which is not acid-quenched, re-

Received Sept. 18, 2009; revised, accepted Oct. 12, 2009.

This work was funded by grants from the National Institutes of Health (5 R01 NS023466) and the Muscular Dystrophy Association (MDA4204). M.A.G. was supported by a National Institutes of Health research training grant (5 T32 NS007083). We thank Steven Fadul for unfailing assistance, Dr. Kristin Schaller for help with genotyping, Dr. Guillermo Alvarez de Toledo and Dr. Rafael Fernandez-Chacón for valuable comments, and Clinton Cave for useful discussions.

Correspondence should be addressed to William J. Betz, Department of Physiology and Biophysics, University of Colorado Denver, RC1 North, P18-7129, P.O. Box 6511, MS 8307, Aurora, CO 80045. E-mail: bill.betz@ucdenver.edu.
DOI:10.1523/JNEUROSCI.4646-09.2009

Copyright © 2009 Society for Neuroscience 0270-6474/09/2915308-09\$15.00/0

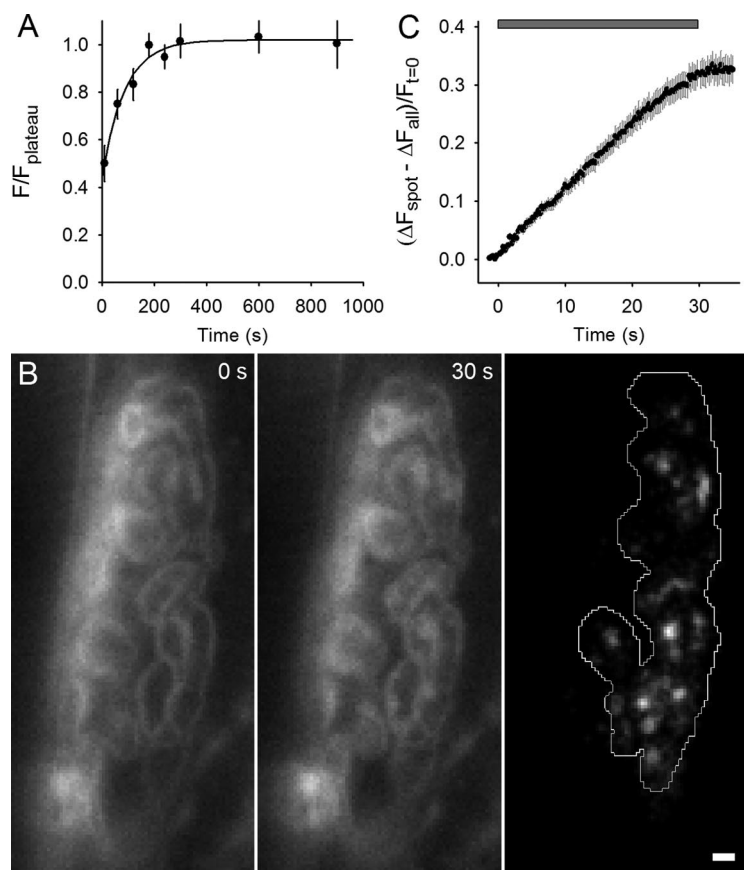


Figure 1. FM4-64 spots appear during 100 Hz stimulation. **A**, Average FM4-64 fluorescence measured versus time in resting terminals. FM4-64 ($3 \mu\text{M}$) was added at $t = 0$. Filled circles indicate measurements and the solid line a single-exponential best fit to the data (time constant = 87 s). Experiments for FM4-64 spot data were started ~ 120 s after dye application. **B**, Left, NMJ in the presence of FM4-64, which shows outline of nerve terminal before stimulation. Middle, Same NMJ after 30 s, 100 Hz nerve stimulation; fluorescent spots have appeared. Right, Difference between middle and left panels revealing FM4-64 spots; the terminal is outlined. Scale bar, $2 \mu\text{m}$. **C**, The change in fluorescence intensity for spots compared with the whole terminal as a fraction of initial fluorescence is plotted versus time. During the time indicated by the gray bar, 100 Hz stimulation was delivered.

mained intact long after stimulation ceased. Thus, the FM4-64 spots, which dissipated only as the nascent endosomes and vesicles dispersed in the cytoplasm, mark endocytosis hot spots. We imaged both fluorophores simultaneously and report that FM4-64 spots arose close to spH spots during intense but not moderate stimulation.

Materials and Methods

Acute muscle preparation. spH mice (Tabares et al., 2007) or wild-type mice (C57BL/6) were housed, handled, and bred in accordance with the University of Colorado Denver Institutional Animal Care and Use Committee. The levator auris longus muscle was dissected from adult mice as described previously (Angaut-Petit et al., 1987) and pinned in a Sylgard-lined chamber. For nerve stimulation, the nerve was drawn into a suction electrode. The perfusing solution contained (in mM) 137 NaCl, 5 KCl, 1.8 CaCl_2 , 1 MgSO_4 , 12 NaHCO_3 , 1 NaH_2PO_4 , and 11 glucose with pH 7.4 and bubbled with 95% O_2 /5% CO_2 . During experiments, gravity fed perfusion was maintained at a rate of ~ 1 ml/min into a volume of ~ 5 ml. Temperature was maintained at $36 \pm 1^\circ\text{C}$ using a dish heater DH-35 and inline heater SF-28 controlled and monitored by a dual automatic temperature controller TC-344B, all from Warner Instruments. Muscle contraction was blocked by adding $3 \mu\text{M}$ curare (Sigma). FM4-64 was added directly to the chamber with an initial chamber concentration of $3 \mu\text{M}$ for characterization experiments. For experiments presented in Figure 3, we used a $1 \mu\text{M}$ concentration after changing filter sets to optimize the FM4-64 signal (see below). The FM4-64 concentration was reduced

again to $0.75 \mu\text{M}$ for Figures 4–7. This reduction did not significantly change the FM4-64 spot characteristics after 100 Hz stimulation (data not shown). To measure synaptic vesicle cluster sizes, terminals were loaded at room temperature with $3.2 \mu\text{M}$ FM4-64 or FM1-43 and stimulated for 1800 shocks at either 10, 30, or 100 Hz. While these stimulation protocols may result in up to a 25% difference in terminal intensity levels (Gaffield and Betz, 2007), all resulted in significantly larger cluster sizes when compared with FM4-64 spots (data not shown). For simplicity, the data for all loading frequencies were pooled for plotting and analysis (Fig. 2B). Electrophysiological recordings (Fig. 3B) were performed as described previously (Gaffield and Betz, 2007). Briefly, we collected miniature end plate potentials and end plate potentials in μ -conotoxin, then calculated quantum content according to Martin (1955).

Imaging and stimulation. Imaging was performed on a Leica DM 4000B microscope with a Leica EL 6000 light source. For the spH signal, we used a Leica L5 filter cube [bandpass (BP) 480/40 excitation, 505 dichroic, and BP 527/30 emission]. For the FM4-64 signal, we used either a Leica N3 filter cube (BP 546/12 excitation, 565 dichroic, and BP 600/40 emission) (Figs. 1, 2) or a Leica TX2 filter cube (BP 560/40 excitation, 595 dichroic, and BP 645/75 emission) (Figs. 3–7). For two-color experiments, the two different channels were collected sequentially with the filter set change taking ~ 500 ms. Images were focused using a $63\times$, 0.9 numerical aperture water-immersion objective from Zeiss. Images were collected using an Andor iXon EM+ DU-897E camera cooled to -55°C and controlled using Andor's Solis Software, version 4.6.5. Pixels were 2×2 binned resulting in 270 nm pixels. For nerve stimulation, trains were generated using an A310 Accupulser and delivered using an A365 Stimulus Isolator, both from World Precision Instruments. Precise timing control between imaging and stimulation was directed from software custom written in Matlab (MathWorks) and sent to the instrumentation via a DAQ Card 6036E and a BNC-2090 board, both from National Instruments.

Image analysis and modeling. All analysis was performed using custom-written Matlab code. Terminals were first masked by hand drawing the terminal outline. Next we subtracted background fluorescence from nonterminal areas. For automated spot detection, we created an image with pixel values indicating the fluorescence change during stimulation ($F_{30s} - F_{0s}$). Then we identified all local peaks (pixels brighter than all eight surrounding pixels). The peaks were sorted by intensity, then, starting with the brightest peak, we identified all connected pixels with at least 75% of the peak's intensity. The resulting pixel grouping became the first spot. This process continued for all of the peaks. If any pixels in a grouping overlapped with another spot (having a brighter peak intensity), then the spot was excluded. Finally, any spots that comprised fewer than three pixels were excluded from further analysis. To find the distance to the nearest terminal edge, we drew an outline of the terminal's edges by tracing the FM4-64 fluorescence observable before stimulation. For nearest-neighbor detection, the center of mass for each identified spot was calculated and then compared with all other centers of mass (for both spots of similar fluorescence and different fluorescence). For randomly generated spot data, spots were randomly placed within terminals whose shapes were taken from actual data and using the spot density calculated for each terminal. Random spots always had a center of mass centered on

a pixel. One thousand spot trials were averaged for each terminal shape to get the average random distribution. The time course of FM4-64 spot dispersion was estimated using linear fits to the recovery phase of both spot and nonspot traces (Fig. 3A). To estimate the amount of exocytosed membrane visible with spH at the end of stimulation, we used end plate potentials and quantal measurements (Gaffield and Betz, 2007) to calculate the number of vesicles fused with each shock. The total release was simply a sum of the total quanta. After fusion, each vesicle was endocytosed and reacidified with a time constant based on spH recovery.

Statistical analysis was performed using Excel (Microsoft), plots and curve fitting were done using SigmaPlot (Systat Software). All experimental conditions were performed on at least three muscles; trial numbers are listed in the text or figure legends. All error bars indicate SEM. Statistical difference was tested using the Student's *t* test with *p* values <0.05 indicating significance.

Results

Imaging of FM4-64 uptake during 100 Hz stimulation reveals fluorescent spots

We used a pipette to add and mix FM4-64 with the normal saline solution in the experimental chamber to a final concentration of $\sim 3 \mu\text{M}$. FM dye fluorescence increases greatly as it partitions into surface membranes and as shown in Figure 1A, the fluorescence of terminals rose with a time constant of 87 s. The preparation was slowly perfused with a solution that did not contain FM dye, so the FM4-64 concentration in the dish became dilute over time. Nerve terminal fluorescence, however, remained steady for at least 10 min (Fig. 1A), during which time experimental measurements were made. Figure 1B (left) shows a typical terminal ~ 2 min after the dye was added. The terminal outline is clearly visible. We then delivered a train of stimuli (100 Hz for 30 s) to the nerve. The image taken immediately after the train (Fig. 1B, middle) shows the emergence of distinct fluorescent spots. The difference image (Fig. 1B, right) shows the spots more clearly. The mean time course of appearance of 84 FM4-64 spots from nine terminals, shown in Figure 1C, revealed a rapid onset with fluorescence accumulating at $\sim 1\%$ of initial intensity levels per second above the terminal average. The rise in fluorescence ended with the end of stimulation.

FM4-64 spots and spH spots have similar characteristics

In experiments involving imaging with one but not both fluorophores, we noted that FM4-64 spots were similar to spH spots in many aspects (Fig. 2A, different preparations). To quantify characteristics, we identified spots using an automatic spot-finding routine (see Materials and Methods). Examples are shown in Figure 2A (bottom). Using this process, we measured several

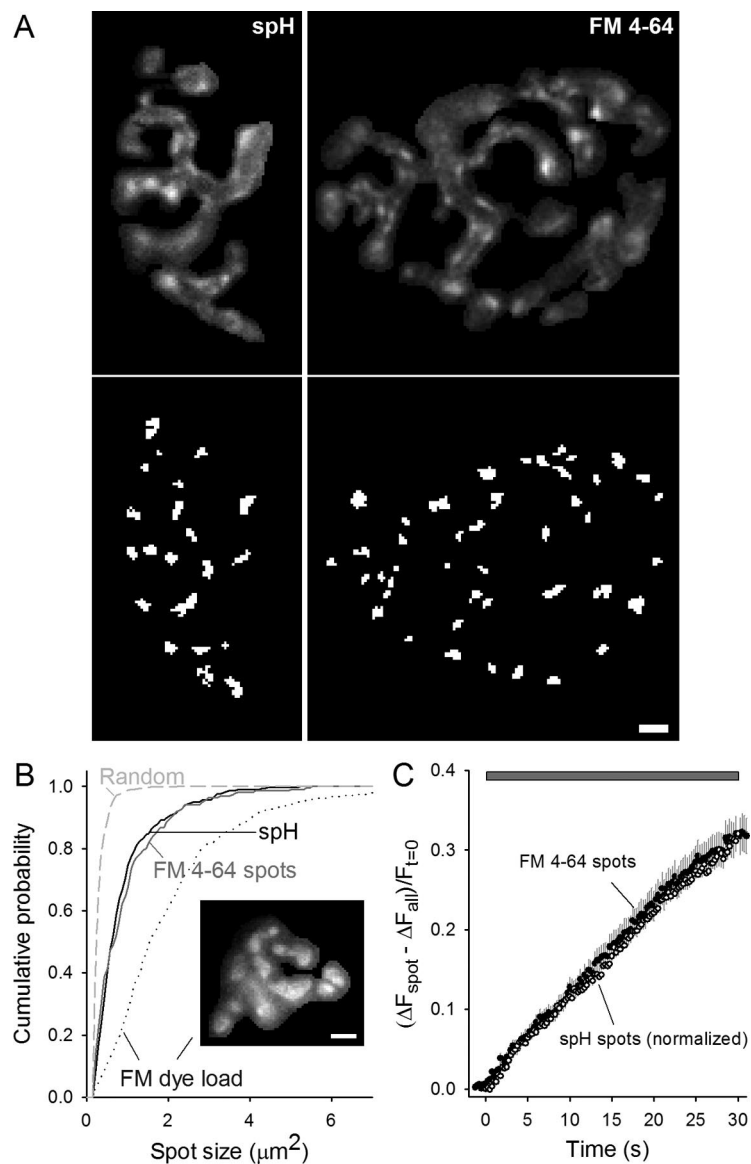


Figure 2. FM4-64 spots and spH spots have similar properties. **A**, Top, Typical difference in spH or FM4-64 fluorescence intensity after a 30 s, 100 Hz stimulation (different preparations). Bottom, Spots identified in the top images by the automatic spot-finding program (see Materials and Methods). Scale bar, $3 \mu\text{m}$. **B**, Cumulative probability plot of spH spot sizes (solid black line) and FM4-64 spot sizes (solid gray line). For comparison to the overall synaptic vesicle population, the synaptic vesicle distribution was assessed after loading with FM dye (dotted line). Inset, A typical FM dye-loaded terminal. The average spot sizes were 0.92 ± 0.05 , 0.98 ± 0.06 , and $2.07 \pm 1.10 \mu\text{m}^2$ for spH spots, FM4-64 spots, and FM dye load, respectively. The dashed line represents the spot size distribution after randomly mixing terminal pixel locations. Data are averaged from 298 spH spots, 220 FM4-64 spots, and 466 FM dye load spots. Scale bar, $3 \mu\text{m}$. **C**, Same plot as Figure 1C with the rise in FM4-64 spot fluorescence shown (filled circles). For comparison, peak spH spot fluorescence was normalized to match the peak FM4-64 spot fluorescence and plotted (open circles). The mean time to half maximum was 14.5 ± 1.3 s and 13.3 ± 0.6 s for spH and FM4-64 spots, respectively ($p = 0.38$, Student's *t* test). The gray bar indicates 100 Hz stimulation.

different spot characteristics. Spot densities were not significantly different (8.9 ± 0.6 per $100 \mu\text{m}^2$ for spH and 8.3 ± 1.1 per $100 \mu\text{m}^2$ for FM4-64). The distances from spots to nerve terminal edges also were not significantly different ($0.75 \pm 0.10 \mu\text{m}$ for spH and $0.77 \pm 0.04 \mu\text{m}$ for spH), nor were they significantly different from randomly placed spots ($0.75 \pm 0.04 \mu\text{m}$). Figure 2B (solid lines) shows that FM4-64 and spH spot sizes were not significantly different. For comparison, the sizes of synaptic vesicle clusters in terminals fully loaded with FM dye are much larger than the spH and FM4-64 spots (Fig. 2B, inset and dotted line). Note that the FM4-64 distribution shown in the solid gray line

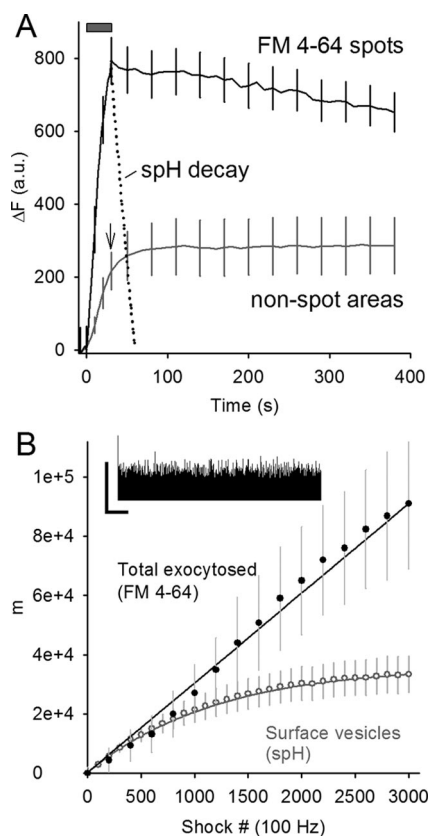


Figure 3. FM4-64 spots persist well after spH endocytosis and reacidification. **A**, Raw change in fluorescence (in arbitrary units) is plotted versus time for either FM4-64 spots (black line) or nonspot areas of the terminal (gray line; arrow marks end of stimulus train). Fluorescence in the FM4-64 spots dispersed slowly after stimulation (train duration indicated by gray bar), particularly when compared with the time course of synaptic vesicle endocytosis and reacidification (spH fluorescence, dotted line). Fluorescence in FM4-64 spots was estimated to match nonspot area fluorescence ~ 17 min after stimulation. Data are averaged from five different terminals. For clarity, error bars are shown for every fifth data point. **B**, spH labels 35% of the vesicles labeled by FM4-64 at the end of 100 Hz stimulation. Inset, Electrophysiological recording of EPPs during 100 Hz stimulation. The vertical calibration bar indicates the peak amplitude of the first EPP, and the horizontal calibration bar indicates 2 s. Main plot, Quanta (m) are plotted versus shock number. The upper solid line indicates the summed quantal release from EPPs. The lower line indicates the “surface vesicles” or those expected to be visible with spH fluorescence based on a simple model using the spH recovery time constant (see Materials and Methods). Actual FM4-64 fluorescence was scaled to match EPP data (filled circles). The gray circles show the average spH fluorescence rise during stimulation after scaling to the theoretical surface vesicle number (lower solid line).

would eventually turn into the dotted line after a 15–20 min wash. Finally, the dashed line in Figure 2B shows the size distribution of “spots” in difference images in which we randomly mixed pixels before running the automatic spot-finding routine. Their much smaller sizes show that the spots that we observed were real, and not simply extracted out of the noise. Figure 2C shows that the time courses of emergence of spH and FM4-64 spots were nearly identical on the time scale of seconds. In summary, FM4-64 and spH spot densities, distances from edge, sizes, and time courses were not significantly different.

FM4-64 spots disperse slowly after stimulation

Figure 3A shows that FM4-64 spots (black solid line) decay much more slowly than spH fluorescence (dotted line; time constant = 12 s). The spH decay reflects internalization of spH, reacidification of synaptic vesicles or endosomes, and quenching of spH. We analyzed 58 total FM4-64 spots identified in five different

terminals and found only one spot with a decay half-time consistent with spH recovery (<30 s). On average, the FM4-64 spots required ~ 15 – 20 min to disperse completely after stimulation ended. As discussed later, the FM4-64 spot decay might reflect the slow budding of vesicles from cisternae, which then move away from the spot into the larger vesicle pool.

The solid gray line in Figure 3A shows the FM4-64 fluorescence change in nonspot regions. The arrow marks the end of the stimulation period. Fluorescence in nonspot areas (which comprised $>90\%$ of the total terminal area) increased slightly after stimulation ended, reaching levels approximating the overall FM4-64 loaded into the terminal. At the end of the stimulus train, the fluorescence in spots accounted for $20.2 \pm 3.1\%$ of the total fluorescence contained within the terminal even though the spots comprised only $6.7 \pm 1.5\%$ of the terminal area, indicating a threefold enrichment of membrane in FM4-64 spot locations.

The majority of vesicles exocytosed during stimulation are internalized by the end of stimulation

At this point we wondered whether the spH and FM4-64 signals should track together. We know that FM dye will partition into any membrane exposed to FM dye in the extracellular solution, thus labeling all exocytosed membrane independently of endocytosis (cf. Smith and Betz, 1996). On the other hand spH fluoresces only when on the surface or in recently endocytosed structures; therefore, the two signals might provide complementary rather than duplicate information. We tested this prediction by calculating the expected difference between the two signals at the end of stimulation—specifically how much exocytosed membrane would be visible with FM4-64 but dark in the spH channel (Fig. 3B).

We first measured the amount of total exocytosis using electrophysiological recordings of end plate potentials (EPPs). The summed quantum contents were then compared with the rate of FM4-64 fluorescence change for the whole terminal. We saw no difference in the exocytosis rate (upper solid line and filled circles, respectively, in Fig. 3B), suggesting that all exocytosed vesicles were labeled by FM4-64. Next, assuming that the time constant of endocytosis/reacidification during stimulation was the same as after stimulation ended (~ 12 s), we estimated that only $\sim 35\%$ of all exocytosed vesicles would be visible in the spH channel at the end of stimulation (Fig. 3B, lower solid line). The actual spH fluorescence change during 100 Hz stimulation (open circles) could be fitted well with this model using a single scaling factor. Comparing the FM4-64 and spH data points at the end of stimulation, the nearly threefold higher FM4-64 signal means that approximately two-thirds of the FM4-64 signal arose from internalized membrane.

spH and FM4-64 spots evoked by intense stimulation colocalize

For the previous experiments, we had imaged spH and FM4-64 spots separately. Naturally, it was of interest to determine whether the spH spots and the FM4-64 spots colocalized, particularly since the signals were similar in so many aspects (Fig. 2), but provided different information on surface and internalized membrane (Fig. 3). We therefore imaged both fluorescence signals simultaneously in the same terminal. To minimize potential interactions between spH and FM4-64, we reduced the FM4-64 concentration to $0.75 \mu\text{M}$. At the end of the stimulus train both spH and FM4-64 spots were visible; four examples are shown in Figure 4. In overlaid images (third column) spH spots (green)

seemed to be in close proximity to a FM4-64 spots (red). For example, point #1 marks an spH spot flanked by two FM4-64 spots. However, there were exceptions. For example, some spH spots appeared without a nearby FM4-64 spot (Fig. 4, point #2), and vice versa (point #3, see Discussion).

We quantified the colocalization in spH and FM4-64 signals in two ways. First, we identified spot locations (Fig. 4, fourth column) and measured the center of mass locations for each spH and FM4-64 spot. We then measured the nearest-neighbor distances for FM4-64 spots to other FM4-64 spots (Fig. 5A, open circles). The nearest-neighbor distribution had a lower limit of $\sim 1 \mu\text{m}$ due to the properties of the automatic spot detection routine (smaller separations were grouped into single spots; see Materials and Methods). For comparison, we randomly placed spots in the terminals (see Materials and Methods) and the average distribution (Fig. 5A, solid gray line) differed little from the observed (dashed lines show 95% interval). Similar results were obtained with spH spots (data not shown). These results suggest that both spH and FM4-64 spots were distributed randomly throughout the terminal. We then measured the nearest-neighbor distribution for FM4-64 spots compared with spH spots (Fig. 5B). In these cases, spot centers could fall within the same pixel because two different spot types were analyzed. The resulting nearest-neighbor distances were considerably smaller than expected by random spot placement (Fig. 5B, compare open circles and solid gray line). Approximately 30% of FM4-64 spots had a corresponding spH spot centered within one pixel's distance (270 nm ; indicated by vertical gray lines in Fig. 5A, B), and 70% of FM4-64 spots had an spH spot within $1 \mu\text{m}$; only 27% of FM4-64 spots would be expected to have an spH spot so close by chance alone.

Our second method for comparing FM4-64 and spH spatial overlap did not rely on spot detection. Instead we sorted each pixel within the terminal (for each fluorescence channel) according to its fluorescence change during the train ($F_{30s} - F_{0s}$). We then calculated the fractional overlap in pixel locations for the two channels as we varied the percentage of total pixels analyzed. The results are plotted in Figure 5C (black line). We found substantially more overlap in FM4-64 and spH fluorescence than predicted by chance (dashed line). For example, the 10% of pixels that brightened the most in each channel (which are a good approximation of the spots themselves) (Gaffield et al., 2009) overlapped $46.5 \pm 3.0\%$, much more than expected by chance (10%). As a test for the quality of the alignment, we shifted the FM4-64 channel by one pixel (x and y) and repeated the calculation. The result (Fig. 5C, solid gray line) showed a small degradation of the colocalization, suggesting that the original alignment was optimal. In summary, during 100 Hz stimulation, spH spots and FM4-64 spots arise at sites scattered randomly throughout the terminal, but in close proximity to one another.

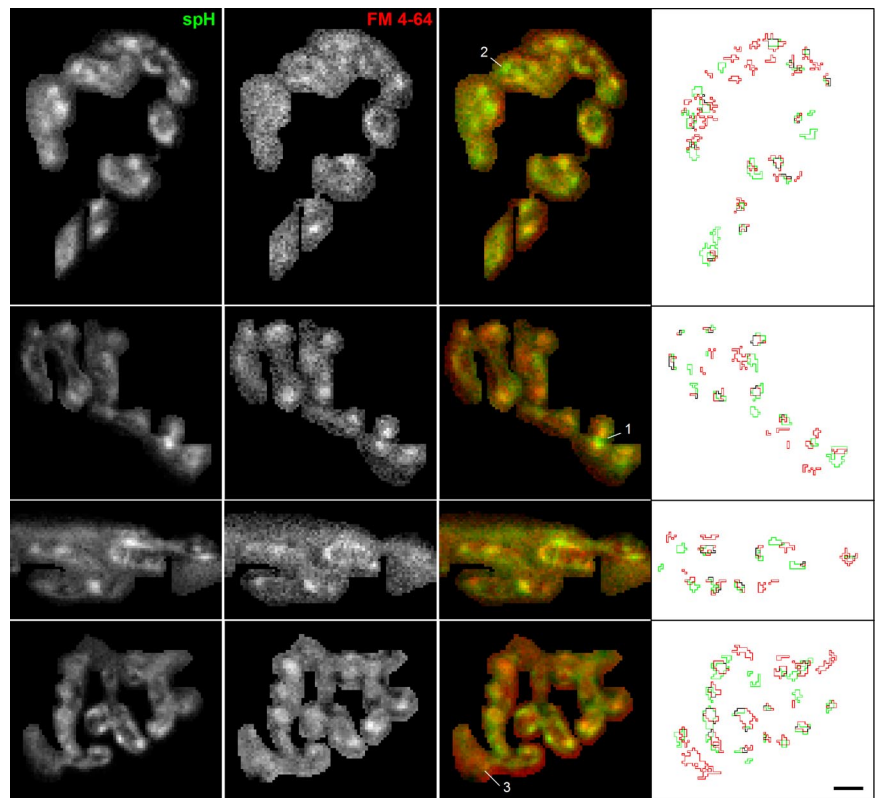


Figure 4. Images show close proximity of spH and FM4-64 spots. Images showing the fluorescence change in response to a 30 s, 100 Hz stimulation measured for both spH (first column) and FM4-64 ($0.75 \mu\text{m}$, second column). The overlay (third column) shows considerably colocalization (yellow). We also number other areas of interest: an spH spot flanked by two FM4-64 spots (spot labeled 1), an spH spot without a nearby FM4-64 spot (spot labeled 2), and an FM4-64 spot without a nearby spH spot (spot labeled 3). The fourth column shows the spot outlines for spH (green) and FM4-64 (red). Scale bar, $3 \mu\text{m}$.

spH and FM4-64 spots are less well correlated at moderate frequencies

We next asked whether spots would colocalize during less intense stimulation (40 Hz instead of 100 Hz). We delivered a 30 s, 40 Hz stimulation train, and collected both spH and FM4-64 fluorescence as before. Two examples are shown in Figure 6. We were able to identify and characterize spH spots after this stimulation (Fig. 6, first column), although they were not as prominent as at 100 Hz. The change in fluorescence in the spots was 1.50 ± 0.04 times the terminal average after 40 Hz stimulation compared with 1.87 ± 0.04 times the terminal average after 100 Hz stimulation ($p < 0.05$, Student's t test). While reducing the stimulation frequency did reduce the spH spot intensity, the spH spot properties were similar to those at higher frequency. The average spot size was $0.80 \pm 0.06 \mu\text{m}^2$ at 40 Hz (compared with $0.92 \pm 0.05 \mu\text{m}^2$ for 100 Hz; $p = 0.13$, Student's t test), and the spot density was 11.33 ± 1.82 per $100 \mu\text{m}^2$ of terminal area (compared with 8.91 ± 0.64 per $100 \mu\text{m}^2$ for 100 Hz; $p = 0.28$, Student's t test). The time constant for spH recovery was 9.6 s after 40 Hz stimulation, modestly faster than after 100 Hz.

In contrast to spH spots, FM4-64 spots were much less evident after 40 Hz stimulation (Fig. 6, second column). The average fluorescence increase in FM4-64 spots was only $5 \pm 0.5\%$ above the initial fluorescence (compared with $32 \pm 2.2\%$ for 30 s, 100 Hz and $14 \pm 1.3\%$ for 12 s, 100 Hz; $p < 0.05$, Student's t test). The average FM4-64 spot size was $3.10 \pm 0.51 \mu\text{m}^2$, over three times the spot size at 100 Hz ($0.98 \pm 0.06 \mu\text{m}^2$; $p < 0.05$, Student's t test), indicating a much more diffuse FM4-64 signal. Consequently, the FM4-64 spot density decreased, although not sig-

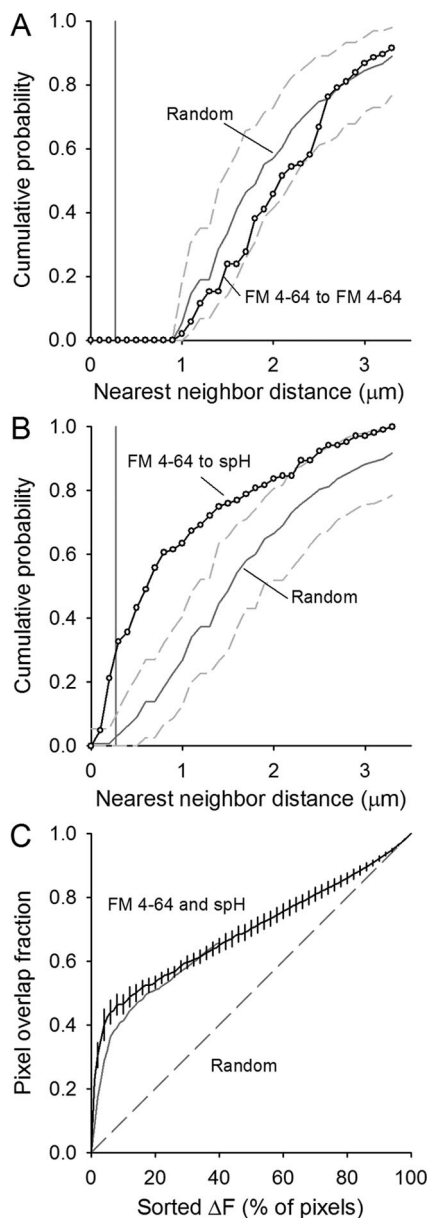


Figure 5. Quantification of spH and FM4-64 spot overlap. **A**, Cumulative probability plot of the nearest-neighbor distances for FM4-64 spots visible after a 30 s, 100 Hz stimulation (open circles). The automatic spot detection prevents any two similar spot types from existing within $\sim 1 \mu\text{m}$ of each other (pixel size = 270 nm, vertical gray line). Spots placed randomly in the terminal (1000 iterations) have an average distribution indicated by the solid gray line with 95% of all random trials falling between the dashed gray lines. Data represent 105 spots from five different terminals. **B**, Cumulative probability plot of the nearest-neighbor distances for FM4-64 spots to spH spots (open circles). Spots centered within one pixel distance lie to the left of the vertical gray line (270 nm). Spots placed randomly in the terminal 1000 times have an average distribution indicated by the dark gray line with 95% of all random trials falling within the dashed gray lines. **C**, For each fluorescent label, the total fluorescence change in each pixel was determined, then pixels were sorted based on their relative fluorescence changes during the 30 s, 100 Hz train. The *x*-axis shows the percentage of those sorted pixels (for example, 10% represents the 10% of all terminal pixels with the largest fluorescence change during stimulation). The overlap in pixel locations for spH and FM4-64 fluorescence is plotted from 0% to 100% (black line with error bars). Overlap is considerably more than by random chance (dashed line). Some of the overlap is lost if the FM4-64 channel is shifted by one pixel in both the *x* and *y* directions (solid gray line), suggesting that the original alignment between the two channels was optimal.

nificantly, to 6.07 ± 1.71 per $100 \mu\text{m}^2$ of terminal area (compared with 8.35 ± 1.12 per $100 \mu\text{m}^2$ for 100 Hz; $p = 0.28$, Student's *t* test).

We tested for colocalization of spH and FM4-64 signals as before. The third column in Figure 6 shows that the spH and FM4-64 signals did not overlap much as indicated by the predominantly green and red color of the overlays. Spot locations also showed considerably less overlap at 40 Hz (Fig. 4, fourth column). In fact, when we quantified the colocalization (Fig. 7), the results were no different from independent and random spacing. We observed a random-like distribution for spH spots alone (Fig. 7A), as with 100 Hz stimulation. In contrast to observations at 100 Hz, however, the spH spots at 40 Hz had an FM4-64 spot nearest-neighbor distribution similar to randomly placing two different spot groups within the terminal (Fig. 7B, compare with Fig. 5B). Finally, the spH/FM4-64 overlap in sorted pixel intensities was much closer to randomness at 40 Hz than at 100 Hz (Fig. 7C, compare with Fig. 5C).

Immediately upon exocytosis of vesicles lacking FM dye, the two fluorescence signals should colocalize as spH fluorescence increases and FM dye partitions into the unlabeled membrane. Thus, we might have expected more colocalization after 40 Hz stimulation. We looked for this extra fluorescence by comparing the change in FM4-64 fluorescence in spH spots to the change in fluorescence of all nonspot areas (neither in spH spots nor in FM4-64 spots). Indeed, we found a 1.25-fold increase. However, even though we could observe the extra signal, we did not identify these fluorescence increases as spots. The reason was that the FM4-64 fluorescence in FM4-64 spots rose 2.76-fold over the rest of the terminal, far above the spH spot locations ($p < 0.05$; Student's *t* test). In other words, the sites of endocytosis at 40 Hz were different from the sites of exocytosis. Thus, the colocalization of spH and FM4-64 hot spots depends on the stimulation frequency, with stronger correlation occurring at higher frequencies.

Discussion

We used two fluorophores (spH and FM4-64) to examine simultaneously the sites of exocytosis and endocytosis in mouse motor nerve terminals. We quantified characteristics of each spot type and found that spH and FM4-64 spots colocalized at high, but not moderate stimulation frequencies. The spH fluorescence indicates surface vesicle levels because vesicle reacidification is much faster (time constant of 1–2 s) (Balaji et al., 2008; Zhang et al., 2009) than our measured recovery time constant of 12 s. Only vesicles yet to complete endocytosis should fluoresce. We have previously provided evidence for spH spots as sites of increased exocytosis (Gaffield et al., 2009). In brief, the spH in spH spots diffused out of the spots into surrounding areas before endocytosis. FM4-64 [a lipophilic dye that fluoresces strongly in lipids (Betz and Bewick, 1992; Betz et al., 1992)], on the other hand, provides a measure of the cumulative amount of exocytosis without regard for the endocytosis state of each vesicle (Smith and Betz, 1996). Because the equivalent of nearly two-thirds of all the exocytosed vesicle membrane was internalized at the end of stimulation (Fig. 3B) [vesicle identity may be lost on the surface (Fernández-Alfonso et al., 2006; Wienisch and Klingauf, 2006; Tabares et al., 2007)], the change in FM4-64 at the end of stimulation preferentially identified endocytosed structures. Ideally, we should be able to match the FM4-64 and spH signals by applying an ATPase inhibitor to prevent vesicle reacidification (Sankaranarayanan and Ryan, 2001), and thus prevent the loss of spH fluorescence. Unfortunately, under our experimental condi-

tions (37°C), we observed a rapid rise in resting vesicle fluorescence shortly after applying the ATPase inhibitor folimycin (see supplemental Fig. 1, available at www.jneurosci.org as supplemental material). As a result, we only observed a weak spH fluorescence response to stimulation.

In the past, FM dyes have been used specifically to label bulk endocytosis (Richards et al., 2000; Clayton and Cousin, 2008). Here, we did not use FM4-64 to specifically label one type of endocytosis over another; rather we probably labeled all fused membrane with FM4-64 (Fig. 3B). Some FM dyes, such as FM2-10, appear to be excluded from bulk endocytosis pathways (Richards et al., 2000). However, at high enough concentrations (100 μM), FM2-10 will also label bulk endocytosis (Clayton and Cousin, 2008). FM4-64 has washout properties similar to FM1-43 (Richards et al., 2000); therefore, FM4-64 should be taken up via all endocytosis pathways.

We explored and compared the nature of the spH and FM4-64 spots by analyzing several different properties during 100 Hz stimulation. The only significant difference was the rate of spot dispersal. During recovery after a stimulus train, spH fluorescence disappeared quickly, indicating both endocytosis and diffusion of spH out of spots ($\sim 50\%$ mobile spH) (Gaffield et al., 2009). FM4-64 spots recovered much more slowly (Fig. 3A), indicating that the majority of the FM4-64 fluorescence increase in these spots was not on the surface. At 100 Hz, due to the strong colocalization of the two signals, we suggest that the majority of endocytosis occurred very near sites of exocytosis. At 40 Hz, however, the majority of FM4-64 was taken up away from spH spots. At 40 Hz we could detect the extra exocytosed membrane at spH spots with FM4-64 (a value of 25% above nonspot areas). We observed an increase in the spH signal of $\sim 50\%$ in spH spots compared with non-spot areas. The difference in these two values (50% in spH fluorescence and 25% in FM4-64 fluorescence) can be attributed to the $\sim 50\%$ mobile spH fraction that might have diffused within the membrane and internalized away from the exocytic spH spots (Gaffield et al., 2009).

FM4-64 spots properties are consistent with other measures of bulk endocytosis

These experiments were performed at physiological temperature (37°C), using physiological stimulation frequencies for type II muscle fibers (Hennig and Lomo, 1985; Erzen et al., 2000), but for nonphysiological durations (30 s, although FM4-64 spots appeared soon after onset of stimulation). The FM4-64 spots identified here are similar in appearance to FM dye spots found in both fly larvae (Kasprowitz et al., 2008) and fixed snake motor nerve terminals after stimulation (Teng et al., 2007). In both cases, the authors explored the nature of these spots using both fluorescence and electron microscopy, determining that FM dye spots labeled bulk membrane retrieval. The size, locations, and time courses of appearance and decay of the FM4-64 spots are also consistent with previous

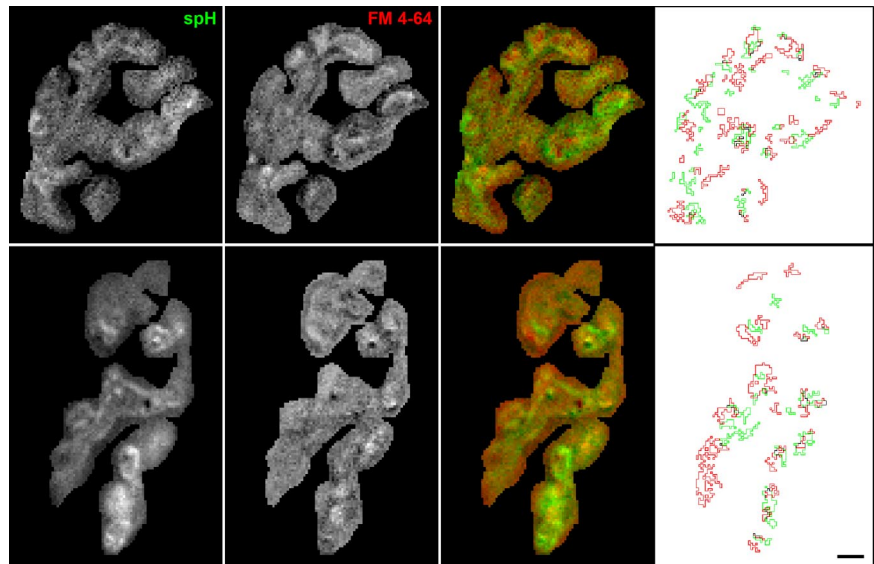


Figure 6. Images show little overlap of spH and FM4-64 spots after moderate stimulation. Images showing the fluorescence change in response to a 30 s, 40 Hz stimulation measured for both spH (first column) and FM4-64 (0.75 μM , second column). The overlay (third column) shows mostly greens and reds with little colocalization (yellow). The fourth column shows spot outlines for spH (green) and FM4-64 (red). Scale bar, 3 μm .

findings on scattered endocytic hot spots in snake motor nerve terminals (Teng et al., 1999). Moreover, the rapid onset of spot appearance is consistent with the time course of bulk endocytosis in central nerve terminals (Clayton et al., 2008). Finally, the slow dissipation of FM4-64 spots, well after complete internalization of synaptic vesicle membrane (provided by the spH signal), is also consistent with the slow regeneration and scattering of synaptic vesicles from structures created by bulk endocytosis (Richards et al., 2000, 2003; Lin et al., 2005), although not necessarily measurements of endosome dissipation (Teng et al., 2007). If the FM4-64 spots were not large endosomes, but rather clusters of synaptic vesicles, then the low mobility of these vesicles would likely make them less fusion competent (Gaffield and Betz, 2007). Snake motor nerve terminals equally relied upon bulk endocytosis at frequencies from 0.3 to 30 Hz (Teng et al., 2007), quite different from our observations in mammalian motor nerve terminals. Possibly, our FM4-64 labeling and spot detection technique preferentially located the largest of cisternae only. Alternatively, endocytosis rates, which are temperature sensitive (Renden and von Gersdorff, 2007; Balaji et al., 2008), might be tuned differently in mammalian and reptilian motor nerve terminals.

We observed prominent endocytosis near the preferred exocytosis sites at 100 Hz stimulation, suggesting that synaptic vesicle membrane was internalized close to highly used release sites. This type of membrane internalization was much less prevalent at 40 Hz. We were still able to identify spH spots during 40 Hz stimulation (albeit at a lower intensity) (see also Wyatt and Balice-Gordon, 2008); therefore, tight spatial control over preferred exocytosis and endocytosis locations must not be required for all stimulation levels. The difference in spH spot intensity at 40 Hz (approximately half that at 100 Hz) may indicate the amount of synaptic vesicle membrane that can be efficiently recovered via non-FM4-64 spot pathways. Future measurements, for example, focusing on noncolocalized spots like those that we noted only anecdotally (e.g., points 2, 3 in Fig. 4), may provide a better idea of the relative exocytosis amounts needed to trigger the appearance of a

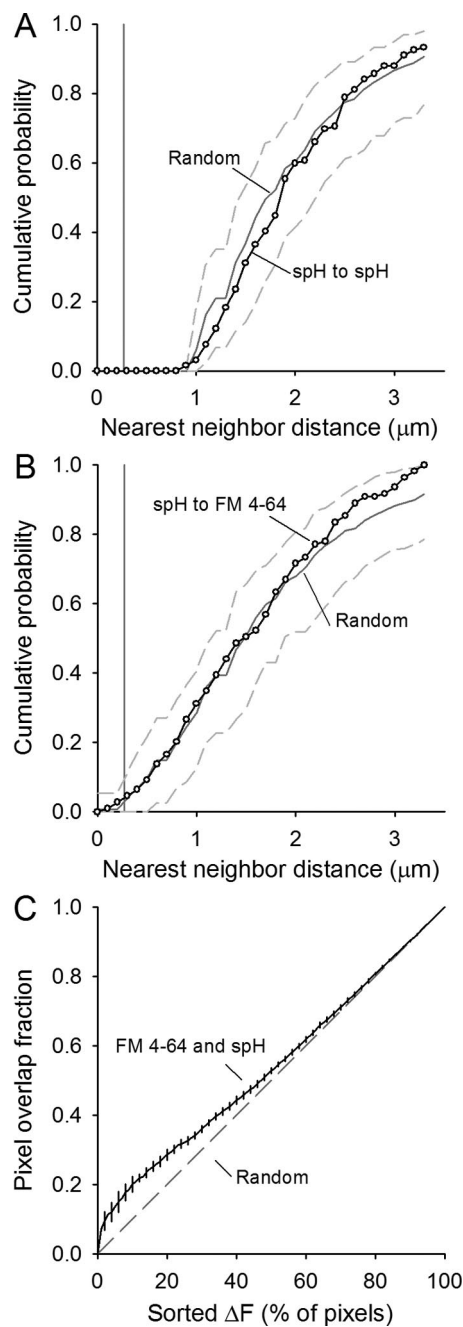


Figure 7. Quantification of spH and FM4-64 spot overlap after moderate stimulation. Plots similar to Figure 5. **A**, Cumulative probability plot of the nearest-neighbor distances for spH spots identified after a 30 s, 40 Hz stimulation (open circles). Data represent 132 spots from four different terminals. Spots placed randomly in the terminal 1000 times have an average distribution indicated by the dark gray line with 95% of all random trials falling within the dashed gray lines. Pixel size is indicated by the vertical gray line. **B**, Cumulative probability plot of the nearest-neighbor distances for spH spots to FM4-64 spots (open circles). Spots placed randomly in the terminal 1000 times have an average distribution indicated by the dark gray line with 95% of all random trials falling within the dashed gray lines. Pixel size is indicated by the vertical gray line. **C**, The overlap in sorted pixel locations for spH and FM4-64 fluorescence is plotted from 0% to 100% of the pixels (black line with error bars). Overlap is only modestly more than expected by random chance (dashed gray line).

nearby endocytic spot. Spatial analysis of other properties related to endocytosis such as intracellular calcium levels (Hosoi et al., 2009), calmodulin activity (Wu et al., 2009), and dynamin I phosphorylation state (Clayton et al., 2009) may help reveal what triggers FM4-64 spot emergence.

A significant number of vesicles cycle through exocytosis/endocytosis hot spots

How important are exocytic and endocytic hot spots in the overall function of the motor nerve terminal? The fluorescence in the spots at the end of stimulation was a good indicator of the spot locations, but not necessarily an indicator of the contribution of a spot to overall synaptic vesicle cycling. For example, some spH signal is lost during stimulation due to rapid endocytosis and reacidification (Gaffield et al., 2009). Factoring in this correction, we estimate that 20–30% of the total spH signal arose in spots even though the spots comprised only 8–9% of the terminal area. For the FM4-64 spots, we provided evidence that 20% of the total FM4-64 fluorescence is located in spot locations at the end of stimulation (Fig. 3A). If we assume that spots disperse at equal rates during and after stimulation, then 20% is a good approximation for the amount of FM dye taken up in the 7% of total terminal area occupied by spots. We cannot rule out that more FM4-64 is taken up via the spot pathway, since vesicles budding from putative endosomes might leave the spots during stimulation. Therefore, 20% is a lower estimate for the amount of membrane uptake via spots at 100 Hz. Consequently, we conclude that both the exocytic pathway visualized by spH spots and the endocytic pathway visualized as FM4-64 spots represent important components of the synaptic vesicle cycle during high-frequency stimulation.

References

- Angaut-Petit D, Molgo J, Connold AL, Faille L (1987) The levator auris longus muscle of the mouse: a convenient preparation for studies of short- and long-term presynaptic effects of drugs or toxins. *Neurosci Lett* 82:83–88.
- Balaji J, Armbruster M, Ryan TA (2008) Calcium control of endocytic capacity at a CNS synapse. *J Neurosci* 28:6742–6749.
- Betz WJ, Bewick GS (1992) Optical analysis of synaptic vesicle recycling at the frog neuromuscular junction. *Science* 255:200–203.
- Betz WJ, Mao F, Bewick GS (1992) Activity-dependent fluorescent staining and destaining of living vertebrate motor nerve terminals. *J Neurosci* 12:363–375.
- Betz WJ, Mao F, Smith CB (1996) Imaging exocytosis and endocytosis. *Curr Opin Neurobiol* 6:365–371.
- Ceccarelli B, Hurlbut WP, Mauro A (1972) Depletion of vesicles from frog neuromuscular junctions by prolonged tetanic stimulation. *J Cell Biol* 54:30–38.
- Ceccarelli B, Hurlbut WP, Mauro A (1973) Turnover of transmitter and synaptic vesicles at the frog neuromuscular junction. *J Cell Biol* 57:499–524.
- Clayton EL, Cousin MA (2008) Differential labelling of bulk endocytosis in nerve terminals by FM dyes. *Neurochem Int* 53:51–55.
- Clayton EL, Evans GJ, Cousin MA (2008) Bulk synaptic vesicle endocytosis is rapidly triggered during strong stimulation. *J Neurosci* 28:6627–6632.
- Clayton EL, Anggono V, Smillie KJ, Chau N, Robinson PJ, Cousin MA (2009) The phospho-dependent dynamin-syndapin interaction triggers activity-dependent bulk endocytosis of synaptic vesicles. *J Neurosci* 29:7706–7717.
- Erzen I, Cvetko E, Obreza S, Angaut-Petit D (2000) Fiber types in the mouse levator auris longus muscle: a convenient preparation to study muscle and nerve plasticity. *J Neurosci Res* 59:692–697.
- Estes PS, Roos J, van der Blik A, Kelly RB, Krishnan KS, Ramaswami M (1996) Traffic of dynamin within individual *Drosophila* synaptic boutons relative to compartment-specific markers. *J Neurosci* 16:5443–5456.
- Fernández-Alfonso T, Kwan R, Ryan TA (2006) Synaptic vesicles interchange their membrane proteins with a large surface reservoir during recycling. *Neuron* 51:179–186.
- Gad H, Löw P, Zotova E, Brodin L, Shupliakov O (1998) Dissociation between Ca²⁺-triggered synaptic vesicle exocytosis and clathrin-mediated endocytosis at a central synapse. *Neuron* 21:607–616.
- Gaffield MA, Betz WJ (2007) Synaptic vesicle mobility in mouse motor nerve terminals with and without synapsin. *J Neurosci* 27:13691–13700.
- Gaffield MA, Tabares L, Betz WJ (2009) The spatial pattern of exocytosis

- and post-exocytic mobility of synaptopHluorin in mouse motor nerve terminals. *J Physiol* 587:1187–1200.
- Hennig R, Lomo T (1985) Firing patterns of motor units in normal rats. *Nature* 314:164–166.
- Heuser JE, Reese TS (1973) Evidence for recycling of synaptic vesicle membrane during transmitter release at the frog neuromuscular junction. *J Cell Biol* 57:315–344.
- Holt M, Cooke A, Wu MM, Lagnado L (2003) Bulk membrane retrieval in the synaptic terminal of retinal bipolar cells. *J Neurosci* 23:1329–1339.
- Hosoi N, Holt M, Sakaba T (2009) Calcium dependence of exo- and endocytotic coupling at a glutamatergic synapse. *Neuron* 63:216–229.
- Kasprowicz J, Kuenen S, Miskiewicz K, Habets RL, Smits L, Verstreken P (2008) Inactivation of clathrin heavy chain inhibits synaptic recycling but allows bulk membrane uptake. *J Cell Biol* 182:1007–1016.
- Koenig JH, Ikeda K (1989) Disappearance and reformation of synaptic vesicle membrane upon transmitter release observed under reversible blockade of membrane retrieval. *J Neurosci* 9:3844–3860.
- Lin MY, Teng H, Wilkinson RS (2005) Vesicles in snake motor terminals comprise one functional pool and utilize a single recycling strategy at all stimulus frequencies. *J Physiol* 568:413–421.
- Martin AR (1955) A further study of the statistical composition on the end-plate potential. *J Physiol* 130:114–122.
- Miesenböck G, De Angelis DA, Rothman JE (1998) Visualizing secretion and synaptic transmission with pH-sensitive green fluorescent proteins. *Nature* 394:192–195.
- Miller TM, Heuser JE (1984) Endocytosis of synaptic vesicle membrane at the frog neuromuscular junction. *J Cell Biol* 98:685–698.
- Ng M, Roorda RD, Lima SQ, Zemelman BV, Morcillo P, Miesenböck G (2002) Transmission of olfactory information between three populations of neurons in the antennal lobe of the fly. *Neuron* 36:463–474.
- Renden R, von Gersdorff H (2007) Synaptic vesicle endocytosis at a CNS nerve terminal: faster kinetics at physiological temperatures and increased endocytotic capacity during maturation. *J Neurophysiol* 98:3349–3359.
- Richards DA, Guatimosim C, Betz WJ (2000) Two endocytic recycling routes selectively fill two vesicle pools in frog motor nerve terminals. *Neuron* 27:551–559.
- Richards DA, Guatimosim C, Rizzoli SO, Betz WJ (2003) Synaptic vesicle pools at the frog neuromuscular junction. *Neuron* 39:529–541.
- Roos J, Kelly RB (1999) The endocytic machinery in nerve terminals surrounds sites of exocytosis. *Curr Biol* 9:1411–1414.
- Sankaranarayanan S, Ryan TA (2001) Calcium accelerates endocytosis of vSNAREs at hippocampal synapses. *Nat Neurosci* 4:129–136.
- Smith CB, Betz WJ (1996) Simultaneous independent measurement of endocytosis and exocytosis. *Nature* 380:531–534.
- Smith SM, Renden R, von Gersdorff H (2008) Synaptic vesicle endocytosis: fast and slow modes of membrane retrieval. *Trends Neurosci* 31:559–568.
- Tabares L, Ruiz R, Linares-Clemente P, Gaffield MA, Alvarez de Toledo G, Fernandez-Chacón R, Betz WJ (2007) Monitoring synaptic function at the neuromuscular junction of a mouse expressing synaptopHluorin. *J Neurosci* 27:5422–5430.
- Takei K, Mundigl O, Daniell L, De Camilli P (1996) The synaptic vesicle cycle: a single vesicle budding step involving clathrin and dynamin. *J Cell Biol* 133:1237–1250.
- Teng H, Wilkinson RS (2000) Clathrin-mediated endocytosis near active zones in snake motor boutons. *J Neurosci* 20:7986–7993.
- Teng H, Cole JC, Roberts RL, Wilkinson RS (1999) Endocytic active zones: hot spots for endocytosis in vertebrate neuromuscular terminals. *J Neurosci* 19:4855–4866.
- Teng H, Lin MY, Wilkinson RS (2007) Macroendocytosis and endosome processing in snake motor boutons. *J Physiol* 582:243–262.
- Wienisch M, Klingauf J (2006) Vesicular proteins exocytosed and subsequently retrieved by compensatory endocytosis are nonidentical. *Nat Neurosci* 9:1019–1027.
- Wu LG, Ryan TA, Lagnado L (2007) Modes of vesicle retrieval at ribbon synapses, calyx-type synapses, and small central synapses. *J Neurosci* 27:11793–11802.
- Wu XS, McNeil BD, Xu J, Fan J, Xue L, Melicoff E, Adachi R, Bai L, Wu LG (2009) Ca²⁺ and calmodulin initiate all forms of endocytosis during depolarization at a nerve terminal. *Nat Neurosci* 12:1003–1010.
- Wyatt RM, Balice-Gordon RJ (2008) Heterogeneity in synaptic vesicle release at neuromuscular synapses of mice expressing synaptopHluorin. *J Neurosci* 28:325–335.
- Xu YF, Autio D, Rheuben MB, Atchison WD (2002) Impairment of synaptic vesicle exocytosis and recycling during neuromuscular weakness produced in mice by 2,4-dithiobiuret. *J Neurophysiol* 88:3243–3258.
- Zhang Q, Li Y, Tsien RW (2009) The dynamic control of kiss-and-run and vesicular reuse probed with single nanoparticles. *Science* 323:1448–1453.